Grid pattern emerging from complex dynamics of defects

Noriko Oikawa,[1,*] Tomohiro Gunji,[2] and Yoshiki Hidaka[2,†]

[1]*Department of Physics and Electronics, Graduate School of Engineering, Osaka Prefecture University, Sakai 599-8531, Japan*

[2]*Department of Applied Quantum Physics and Nuclear Engineering, Faculty of Engineering, Kyushu University, Fukuoka 819-0395, Japan*

(Received 30 May 2018; revised manuscript received 29 March 2020; accepted 27 April 2020; published 4 June 2020)

The formation process and growth dynamics of the grid pattern, a cellular convective pattern in the electroconvection of nematic liquid crystals, are investigated. The grid pattern appears via a disordered state called defect turbulence with the increasing of an applied voltage. The averaged defect density increases with the applied voltage and then the defects that have been in the continuous process of creation and annihilation are frozen as grid cells forming domain structures. The area fraction of the grid domains is adopted as the order parameter. The temporal growth of the area fraction for the step voltage was also measured. By applying the Kolmogorov-Avrami model to the results, it is suggested that the growth dynamics of the grid domain is not primarily governed by domain growth, but by the local transition of the rolls to the cellular flow via preliminary grid structures that transiently appear.

DOI: 10.1103/PhysRevE.101.062204

I. INTRODUCTION

In nonequilibrium open systems, a variety of spatial patterns with different symmetries appear [1,2]. One of the typical examples of nonequilibrium open systems is a convective system. In spatially extended convective systems, generally, various spatial patterns appear resulting from successive bifurcations with increase of the control parameter. In this picture of pattern formation, a new unstable mode with short wavelength grows from thermal fluctuations at the bifurcation point. Therefore, a pattern which appears via a bifurcation has lower symmetry than the previous one. In theoretical approaches, it is noted that this new mode has a long characteristic time near the transition point. Based on the slaving principle [3], convection pattern formation is described as the dynamics of this mode, that is, the amplitude equation [4]. This approach has been considered to be available for the formation of higher-order patterns as well as for the formation by the primary instability.

Such aspect of pattern formation is similar to the structural phase transition due to the excitation of a soft mode with a decrease of temperature in equilibrium systems [5]. Namely, the new mode in a convective system is also recognized as a kind of a soft mode below the bifurcation point [6]. This corresponds to the fact that the amplitude equation describing the pattern formation of the convection system can be categorized in the Ginzburg-Landau theory. For nonequilibrium open systems such as convective systems, although free energy cannot be defined, the dynamics of the new mode is represented by the variation of a potential (Lyapunov function) [4]. The similarity to the phase transitions is also found in the dynamics of the pattern formation. The formation dynamics of a convective pattern after a jump of the control parameter across the threshold [7,8] is reminiscent of the ordering processes of the lower-symmetry structures after quenching of the temperature across the phase transition point [9,10]. Namely, the amplitude of the pattern grows homogeneously in the whole system. Although incoherence of the phase of the pattern exists in the beginning, the spatial variation of the phase slowly diffuses and the system eventually reaches a complete ordered state. Thus, it seems that pattern formation in nonequilibrium open systems and phase transition in equilibrium systems possess some overlaps in their behaviors and the interpretations. However, nonequilibrium dissipative systems showing temporal behavior such as limit cycles and chaos generally have no potential function which determines the stationary states of the system with its minima. Therefore, bifurcation in nonequilibrium open systems is generally considered to be more complex than that in equilibrium systems.

Compared to convective systems of isotropic fluids, electroconvective systems of nematic liquid crystals have more variety of spatial patterns due to the additional degree of freedom brought by the anisotropy of the nematic director [11,12]. In the electroconvective system, a grid pattern (GP) is formed in a wide range of the relevant parameter [13]. The GP is characterized by a cellular convective structure with an additional wave vector perpendicular to the primary rolls pattern (normal rolls). Although the GP has been known as a typical higher-order pattern, the typical formation scenario in which a new soft mode appears from thermal fluctuations does not apply to its formation process. With an increasing of an applied voltage, the GP appears via a disordered state in which defects exhibit complex dynamics. This is in contrast to the usual case of transitions of the pattern formation, in which the pattern develops towards states that have lower symmetries. In addition, the GP appears in an island shape in the disordered state. Considering these aspects, the analogy

*oikawa@pe.osakafu-u.ac.jp
†hidaka@ap.kyushu-u.ac.jp

with the emergence of the soft modes in equilibrium systems does not seem to be applicable to the formation of the GP.

It is known that the Kolmogorov-Avrami (KA) model successfully describes the dynamics of nucleation and domain growth in the crystal growth [14]. The model does not depend on the microscopic physical process of the system. Therefore, the KA model could be used to analyze nonequilibrium open systems [15] as well as other material systems [16] if the transition from an unstable state to another stable state occurs through nucleation and domain growth. It is expected that by applying the KA model to the temporal growth of the area fraction of the GP, the formation mechanism of the GP can be discussed from the viewpoint of nucleation and domain growth. Despite a number of studies on the GP [11,17–20], the formation scenario and the dynamics of the GP have not yet been sufficiently explained. It is not clear how the system enters into the ordered state suppressing the chaotic motions of defects. In this paper, the formation and growth dynamics of the GP have been experimentally investigated by defining an order parameter of the GP state.

II. EXPERIMENT

We used the nematic liquid crystal *p*-methoxybenzilidene-*p'*-*n*-butylaniline (MBBA), which was filled into the space between two parallel glass plates. The separation between the two glass plates was maintained by a polymer spacer. The surfaces of the glass plates were coated with transparent electrodes (indium tin oxide) of size $1.0 \times 1.0\ \mathrm{cm}^2$. In order to realize the planar alignment of nematics in the x-y plane which is parallel to the glass plates, the surfaces of the glass plates were rubbed in one direction (defined as the x direction) after treatment of a surfactant (polyvinyl alcohol). The liquid crystal was doped with tetra-*n*-butyl-ammonium bromide (TBAB) in order to control electric conductivity. The experimental temperature was controlled at $30.00 \pm 0.03\ ^\circ\mathrm{C}$ by using a control system that consists of a Ni-Cr-wire heater, Pt resistance, and a proportional-integral-differential (PID) regulator. The relative dielectric constant of the sample cell was $\epsilon_\perp = 4.8$ and the electric conductivity was $\sigma_\perp = 1.1 \times 10^{-7}\ \Omega^{-1}\,\mathrm{m}^{-1}$. The thickness of the sample cell was $d = 29.3\ \mu\mathrm{m}$. Thus, the aspect ratio of the convective system was $\Gamma = 341$. The sample cell was observed in a polarizing microscope (Nikon) equipped with an insulated hot stage. An ac voltage $V_{\mathrm{ac}}(t) = \sqrt{2}V\cos(2\pi f t)$ was applied to the sample in the z direction using a digital synthesizer (NF1946). The frequency f was set to 300 Hz. The image data were taken by a charge coupled device (CCD) camera (HAMAMATSU C4880-80) mounted on the microscope. The observation area was $36.3d \times 27.4d$ and the image was digitized with the size of 656×494 pixels. The self-made software was used for the image analysis.

III. RESULTS AND DISCUSSION

A. Formation scenario

When the applied voltage is increased, normal rolls begin to fluctuate beyond a threshold voltage. Consequently, defects (dislocations) of the rolls' pattern appear and exhibit complex dynamics. The defects are randomly created in space and time

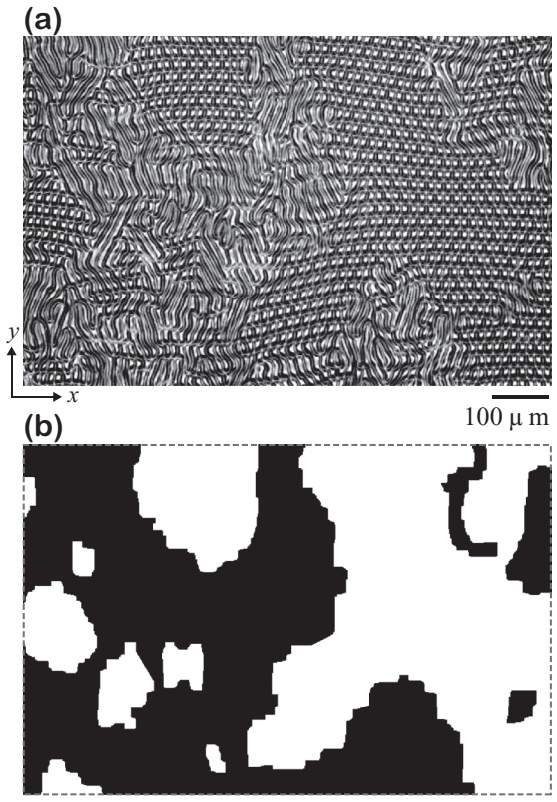

FIG. 1. (a) Image of the coexistence of a GP and a disordered state called defect turbulence. (b) Binary picture obtained by the image processing for (a), where white and black regions indicate the GP and the defect turbulence, respectively. The image represents a state in $F_\eta = 50\%$.

and actively glide through the system. When a defect collides with another one that has the opposite sign, both the defects annihilate. With further increasing the voltage, the transition to GP occurs locally, whereas in the other area complex dynamics of defects still remain, as shown in Fig. 1(a). That is, the GP state and the disordered state coexist during the transition process to the GP. At a constant voltage, the GP domains do not largely deform. Therefore, it is considered that the area fraction of the GP is an appropriate order parameter of the formation of the GP. A snapshot image was divided into a GP and disordered state by detecting the characteristic wave number q_{GP} of the GP in the y direction by using Fourier image analysis [see Fig. 1(b)] [21,22]. The area fraction of the GP was defined as $F_\eta = S_{\mathrm{GP}}/S_0$, where S_{GP} and S_0 indicate the total GP area and the whole observed area, respectively. The applied voltage V was increased with a step of $0.2V$, and the image was recorded after a waiting time of 5 min in each voltage increase. Figure 2 shows the dependence of the area fraction of the GP on the normalized voltage, $\eta = (V^2 - {V_{\mathrm{GP}}}^2)/{V_{\mathrm{GP}}}^2$. V_{GP} indicates the voltage beyond which S_{GP} becomes $S_{\mathrm{GP}} > 0$. F_η increases with η to the maximum value of $\sim 80\,\%$, and turns to decrease as the GP gradually dissolves into a turbulent state. Finally, the whole system reaches the turbulent state (dynamic scattering mode 1).

To understand the transition to the GP, it is important to perceive the origin and the intrinsic properties of the complex

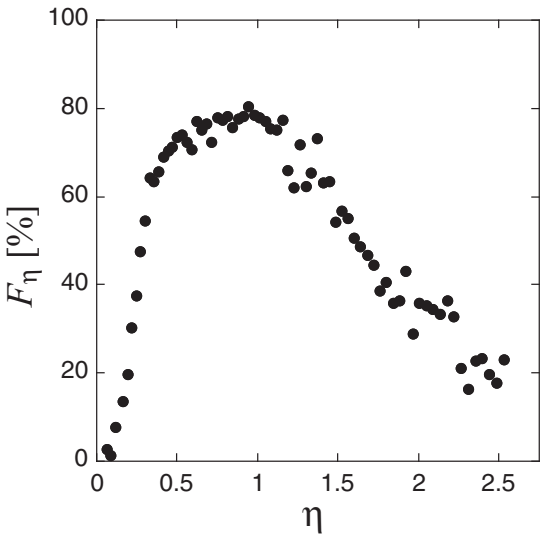

FIG. 2. Dependence of the area fraction F_η of the GP on the normalized voltage η.

dynamics of defects. It is thought that the mechanism of generation and the dynamics of defects can be explained by the following. In the electroconvective effect, convection occurs such that the direction of the wave vector of the convective rolls' pattern is parallel to the director of the nematic liquid crystals. On the other hand, the two-dimensional director **C**, which is the projection of nematic director **n** onto the x-y plane, is constantly subjected to viscous torque from the convective flow [23]. When ε is relatively small, the rotation of the director due to the torque is suppressed by the planar anchoring. Thus, the normal rolls are kept stable. When ε is beyond a threshold value, however, the director rotates, surmounting the anchoring. This rotation also makes the convective wave vector rotate because its direction prefers to be parallel to the nematic director by the electroconvective effect. The azimuths of the **C** director and the convective wave vector form an activator-inhibitor system, which causes the Hopf instability due to frustration between the viscous torque and the electroconvective effects. In small convective systems of which the aspect ratio is $O(1)$, this instability appears as a limit-cycle oscillation in the angle of the convective wave vector [24]. In convective systems with large aspect ratio, on the other hand, this instability occurs incoherently in space and time. The rotation of the convective wave vector leads to the skewed varicose instability and the zigzag instability [25], and, consequently, defects in the rolls' pattern are randomly created in space and time. This state appearing in large systems has been traditionally called defect chaos or defect turbulence [26,27]. In the defect turbulence, since the randomly created defects largely glide in the system, limit-cycle oscillation is not observed clearly, unlike the small systems. However, recent research has revealed that oscillatory components are included in the dynamic structure factor of the defect turbulence [28].

It is revealed from detailed observations that the formation of the GP occurs in the following steps. When V is increased to an adequately higher value from the threshold voltage of the defect turbulence, oscillation between two convective modes of $\mathbf{q}_1$ and $\mathbf{q}_2$, which are reflection symmetric to the x direction, begins to occur locally, as shown in Fig. 3 [11,29,30]. During the change from $\mathbf{q}_1$ to $\mathbf{q}_2$, both the $\mathbf{q}_1$ and $\mathbf{q}_2$ modes transiently coexist. In the coexistent state, due to the modulation with $\mathbf{q}_2 - \mathbf{q}_1$, defects are created by the pinching of rolls along the modulation lines, as also reported in Ref. [11]. At the instant when the amplitudes of $\mathbf{q}_1$ and $\mathbf{q}_2$ become the same magnitude, a cellular structure appears by superposition of $\mathbf{q}_1$ and $\mathbf{q}_2$, as shown at the center in Fig. 3. Hereafter, this state is called "pre-GP." The pre-GP appears only transiently in time and locally in space. With further increase of V, the tilt angles of $\mathbf{q}_1$ and $\mathbf{q}_2$ with respect to the x direction become larger and the wave number $|\mathbf{q}_2 - \mathbf{q}_1|$ of the modulation also becomes larger. As the wave number $|\mathbf{q}_2 - \mathbf{q}_1|$ increases, the distance between defects decreases and the averaged defect density increases in the defect turbulence, as shown in Fig. 4 [30]. When V is beyond V_{GP}, the oscillation of the local wave vector ceases and the pre-GP freezes to a new stable state, stationary GP, which is the GP being focused on here. In the GP, the structure of the convective flow changes to cellular [11]. This cellular convection could be recognized as a metastable state that has a characteristic wave number q_{GP} in the y direction. Therefore, it is considered that the pre-GP changes to the stationary GP when the y component of the $\mathbf{q}_1$ (and $\mathbf{q}_2$) becomes equal to q_{GP} by an increase of V.

The stationary grid state and the related oscillation of the convective rolls are also observed in other systems [31,32]. However, the GP is formed in a strongly nonlinear regime differently from those systems in which the parameter is restricted in the weakly nonlinear regime just beyond the convective threshold.

Since, as mentioned above, the defect is created at the point where the roll is pinched, as seen in Fig. 3, a grid point of the GP corresponds to a defect. It is thought that the reason why the increasing rate of the defect density changes at $\eta = 0$ in Fig. 4 is because the defects that have been in the continuous process of creation and annihilation in the defect turbulence are frozen and no longer vanish when the GP is formed.

In the region of the defect turbulence, the variance of the distances among defects is relatively large. Inside the GP domain, in contrast, it is considered that the defects arrange periodically and the distances between neighboring defects are almost constant since a grid point corresponds to a defect, as mentioned above. In addition, as shown in Fig. 5, it is confirmed that the averaged area occupied by a grid point in the GP region stays constant for increasing V, even though the averaged area occupied by a defect for the defect turbulence region continues decreasing. Thus, it can be assumed that the GP has a close-packed structure of the defect.

In the present case, the transition to the stationary GP occurs locally and the other area stays in the defect turbulence or pre-GP structure, as shown in Fig. 1. Thus, the long correlation length associated with a transition that arises with the soft mode is not recognized in the formation process of the GP. From this observation, it seems that the GP is not formed by the soft-mode-like mechanism, but by the local transition of the convective structure. The domain structure of the GP is analogous to that of the crystal growth from nucleation in supersaturated solutions. In this analogy, defects and GP cells in the present system, respectively, correspond to dissociation

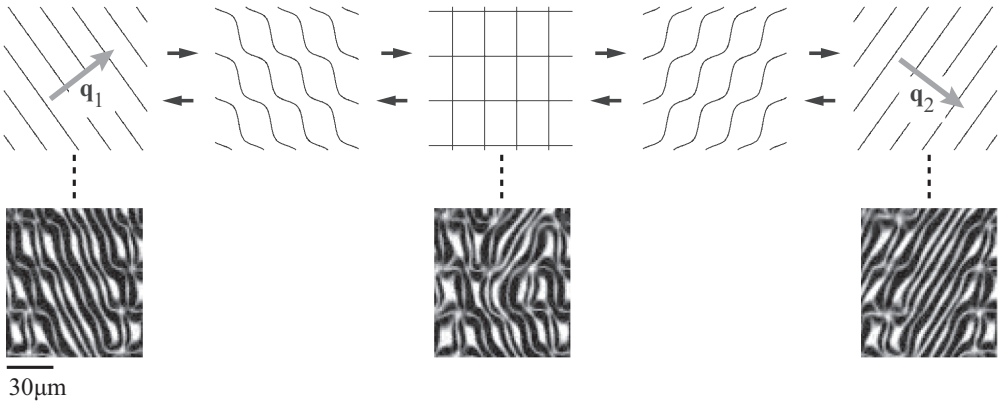

FIG. 3. Schematic representation and the corresponding images of oscillation between the two convective modes, $\mathbf{q}_1$ and $\mathbf{q}_2$.

and crystallization of monomers in the crystal growth. And the area fraction F_η of the GP, which is the order parameter in the GP formation, corresponds to the degree of crystallinity, which is the order parameter characterizing the state in the crystal growth.

B. Growth dynamics

As mentioned in Sec. I, the dynamics of nucleation and domain growth as seen in the crystal growth can be described by the KA model. According to the model, the growth dynamics of the area fraction of a state which spreads from nuclei in a two-dimensional system is described by

$$\frac{S(t)}{S_0} = 1 - \exp\left[-\int_0^t J(\tau)\sigma(t,\tau)d\tau\right], \tag{1}$$

where $S(t)$ and S_0 are the area of the solid state and the whole system, respectively. Here, $\sigma(t,\tau)$ is the area of the state that spreads from a nucleus generated at time τ and expressed as $\sigma(t,\tau) = \pi\{r_c + v(t)(t-\tau)\}^2$, where r_c and $v(t)$ are the nucleus radius and the velocity of a domain front, respectively. $J(\tau)$ is the nucleation rate. If $J(\tau)$ and $v(t)$ are assumed to be constant, then a simple formula,

$$\frac{S(t)}{S_0} = 1 - \exp\left\{-\frac{\pi J_0}{3v_0}\left[(r_c + v_0 t)^3 - r_c^3\right]\right\}, \tag{2}$$

is obtained from Eq. (1), where J_0 and v_0 are the constant nucleation rate and the constant front velocity, respectively.

For the present case, the left-hand side of Eq. (2) should be $F(t)/F_\infty$, where $F(t)$ indicates temporal growth of the area fraction of the GP, and F_∞ is the area fraction in saturation at each value of the voltage, which corresponds to F_η in Fig. 2. In the case of the turbulence-turbulence (dynamic scattering mode 1-2) transition in electrohydrodynamic systems of nematic liquid crystals, it has been reported that the nucleus radius r_c can be assumed to be zero, similar to most of the cases of crystal growth because the size of the nucleus is microscopic [15]. In the present system, in contrast, the pre-GP structures transiently exist just below the threshold V_{GP} and play a role of nucleus in the growth dynamics. Therefore, r_c remains a finite value. Thus, Eq. (2) should be

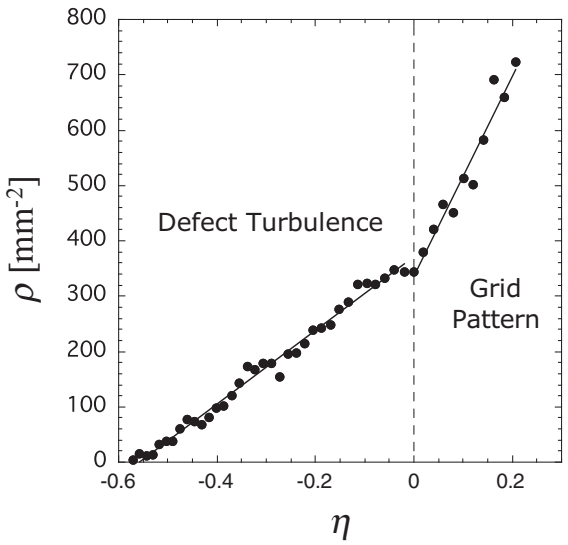

FIG. 4. Dependence of the defect density ρ on the normalized voltage η. A grid point of the GP and the pre-GP is regarded as a defect. The number N_d of defects (including grid points of the pre-GP) in the defect turbulence region and the number N_g of grid points in the GP region were measured in a snapshot recorded at each value of η. ρ is defined as $\rho \equiv (N_d + N_g)/S_0$.

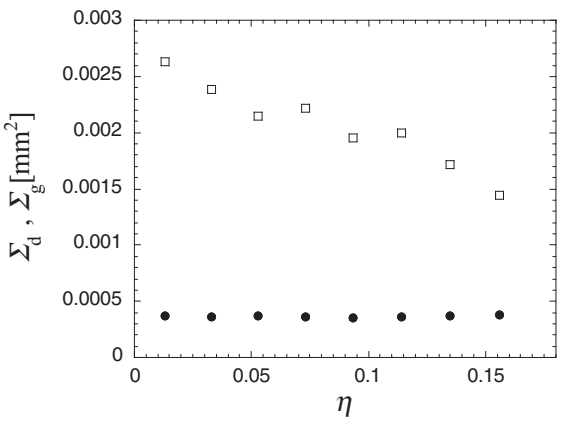

FIG. 5. Dependence of the averaged area occupied by a defect on the normalized voltage η. $\Sigma_d \equiv (S_0 - S_{GP})/N_d$ (open square) and $\Sigma_g \equiv S_{GP}/N_g$ (closed circle) indicate the averaged area occupied by a defect for the whole defect turbulence region and the averaged area occupied by a grid point for the whole GP region, respectively.

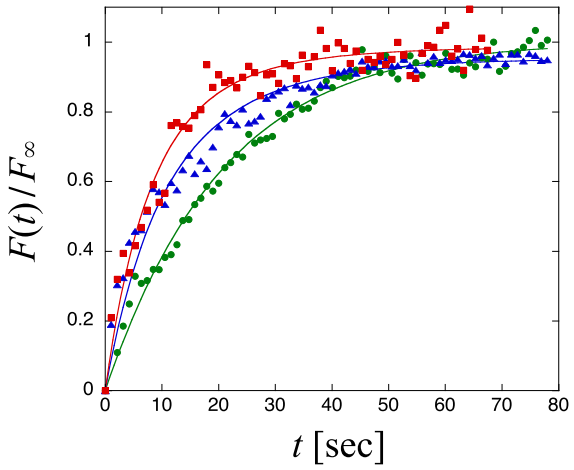

FIG. 6. Temporal growth of the area fraction $F(t)$ of the GP scaled by the saturated value F_∞ of $F(t)$ for $\eta = 0.50$ (green circles), 0.92 (blue triangles), and 1.35 (red squares). The solid lines represent least-squares fittings with Eq. (3).

transformed to

$$\frac{F(t)}{F_\infty} = 1 - \exp\left\{-\frac{\pi J_0^*}{3v_0^*}[(1+v_0^* t)^3 - 1]\right\}. \qquad (3)$$

Here the new parameters are introduced as $J_0^* = J_0 r_c^2$ and $v_0^* = v_0/r_c$ for the sake of decreasing the number of the parameters.

In order to compare the growth dynamics of the GP with Eq. (3), we measured the temporal growth of the area fraction $F(t)$ of the GP for step voltages. The applied voltages were jumped from a value slightly below V_{GP} to different values above V_{GP} at $t = 0$. The values chosen are $\eta = 0.50$, 0.92, and 1.35, which are below the peak of F_η with respect to η (see Fig. 2), almost at the peak, and beyond the peak, respectively. Temporal growth $F(t)$ of the area fraction of the GP was calculated from the sequences of the images taken with a time interval of 1.05 sec by using the method introduced in Sec. III A to obtain F_η.

Each $F(t)$ monotonously increased and saturated to a final value. The saturation value F_∞ obtained by least-squares fitting of $F(t)$ with Eq. (3) was 59%, 82%, and 54% for $\eta = 0.50$, $\eta = 0.92$, and $\eta = 1.35$, respectively. The results of $F(t)/F_\infty$ are shown in Fig. 6. The solid lines indicate least-squares fittings with Eq. (3).

Here, r_c is assumed to be independent of η because it corresponds to the size of the pre-GP that appears below the threshold V_{GP}. The resulting values of J_0^* and v_0^* are shown in Table I. From the fact that J_0^* increases systematically with η, it is thought that the dependence of the growth rate of $F(t)$ on η observed in Fig. 6 is led by the effect of J_0^*. On the other hand, v_0^* have extremely small values for all the values of η. The minus signs of the v_0^* likely came from the fitting errors. Judging from the small values of the front velocity, domain growth is not a primary process in the formation dynamics of the GP for step voltage. This indicates that aggregation of the defects seldom occurs. In the experimental observations, the GP was formed locally by freezing of the incessant motion of the rolls seen in Fig. 3. Thus it may be concluded that the formation of the GP is not governed by domain growth dynamics, but by the local transition of the rolls to cellular flow in the turbulent bulk. For example, molecules in the crystal growth tend to aggregate regularly to reduce the chemical potential. In contrast, in the formation of the GP, which occurs in a nonequilibrium open system, such potential energy governing the state of the whole system cannot be defined. This could be one of the reasons why aggregation of the defects seldom occurs.

TABLE I. Resulting fitting values of the experimental data obtained by the least-squares fit of $F(t)$ shown in Fig. 6 with Eq. (3).

η	J_0^* (1/sec)	v_0^* (1/sec)
0.50	0.015	0.00078
0.92	0.028	−0.010
1.35	0.037	−0.0094

IV. CONCLUSION

The formation and the growth dynamics of the GP emerging from the defect turbulence, in which defects exhibit complex dynamics, have been investigated. In the defect turbulence, the averaged defect density increases with the applied voltage and, when the distance between defects sufficiently decreases, the local convective structure transforms from rolls to cellular flow. The cellular structure first appears transiently in time and locally in space as pre-GP. For further increasing of the applied voltage, the pre-GP becomes stationary GP. Since the GP has domain structure and the pre-GP structure plays a role of nucleus, the GP formation seems to be analogous to the crystal growth in supersaturated solutions. The temporal growth of the area fraction of GP for step voltages was measured in order to compare the domain growth dynamics of the GP with the Kolmogorov-Avrami model. By applying the Kolmogorov-Avrami model to the experimental results, we found that the growth dynamics of the GP for the step voltage is not described as a domain growth phenomena, but rather governed by a local transition from the rolls to the GP.

As mentioned in Sec. I, the soft mode plays an important role in the theoretical approaches for the convective pattern formation. However, in the case where two or more states coexist, other approaches are desired. Such coexistent state often appears in the transition between the ordered state and the disordered one in nonequilibrium open systems. The system in which the two states are separated by a well-defined boundary is called spatiotemporal intermittency (STI) [33–36]. In the STI, the shape of the boundary and the area fractions of the both states fluctuate in space and time. The coexistence of the stationary grid structures and the defect turbulence in the present system is regarded as an STI one. From recent progress in the studies of the STI, it has been accepted that the transition to turbulence in shear flows is described by the directed percolation model [37–40]. However, since the ordered state emerges from the disordered state in the present system in the transition to the GP, it is thought that the GP should be regarded as a different type of STI from the above ones.

One may also think of exploiting the concept of metastability for the coexistence of the two states. Usually alternation of the stabilities of two states can be represented by deformation of the double-well potential, which is induced by a change of the control parameter and, subsequently, the subcritical transition is realized. A Langevin-type equation with a potential function and a random force may be suitable to describe the transition of the present GP system [41]. It is expected that the construction of such type of phenomenological model provides a hint for further understanding of STI and brings a different concept to the field of pattern formation.

ACKNOWLEDGMENTS

This work was supported by JSPS KAKENHI (Grants No. JP15K05799, No. JP25103006, and No. JP17K14356).

[1] M. C. Cross and P. C. Hohenberg, Pattern formation outside of equilibrium, Rev. Mod. Phys. **65**, 851 (1993).
[2] M. Cross and H. Greenside, *Pattern Formation and Dynamics in Nonequilibrium Systems* (Cambridge University Press, Cambridge, 2009).
[3] H. Haken, *Synergetics*, 3rd ed. (Springer, Berlin, 1983), pp. 191–227.
[4] H. Mori and Y. Kuramoto, *Dissipative Structures and Chaos* (Springer, Tokyo, 1998), Chap. 1.
[5] L. D. Landau and E. M. Lifshitz, *Statistical Physics, Part 2*, 3rd ed. (Butterworth-Heinemann, Oxford, 1980).
[6] I. Rehberg, S. Rasenat, M. de la Torre Juarez, W. Schopf, F. Horner, G. Ahlers, and H. R. Brand, Thermally Induced Hydrodynamic Fluctuations Below the Onset of Electroconvection, Phys. Rev. Lett. **67**, 596 (1991).
[7] Y. Hidaka, H. Orihara, Y. Miyazaki, T. Nagaya, and Y. Ishibashi, Dynamics of one-dimensional periodic pattern formation on the electro-hydrodynamic convection of a nematic liquid crystal, J. Phys. Soc. Jpn. **65**, 64 (1996).
[8] Y. Hidaka, Study on the dynamics of nonlinear nonequilibrium patterns in liquid crystals, Ph.D. thesis, Nagoya University, 1995.
[9] H. Orihara, M. Nakamura, and Y. Ishibashi, Temporal evolution of patterns in quenched twisted-nematic cells -dynamics and fractal-, J. Phys. Soc. Jpn. **59**, 2355 (1990).
[10] T. Nagaya, H. Hotta, H. Orihara, and Y. Ishibashi, Experimental study of the coarsening dynamics of $+1$ and -1 disclinations, J. Phys. Soc. Jpn. **61**, 3511 (1992).
[11] A. Joets and R. Ribotta, Hydrodynamic transitions to chaos in the convection of an anisotropic fluid, J. Phys. (Paris) **47**, 595 (1986).
[12] S. Kai, K. Hayashi, and Y. Hidaka, Pattern forming instability in homeotropically aligned liquid crystals, J. Phys. Chem. **100**, 19007 (1996).
[13] K. Hirakawa and S. Kai, Analogy between hydrodynamic instabilities in nematic liquid crystal and classical fluid, Mol. Cryst. Liq. Cryst. **40**, 261 (1977).
[14] M. Avrami, Kinetics of phase change. I General theory, J. Chem. Phys. **7**, 1103 (1939).
[15] S. Kai and W. Zimmermann, Pattern dynamics in the electrohydrodynamics of nematic liquid crystals, Prog. Theor. Phys. Suppl. **99**, 458 (1989).
[16] Y. Ishibashi and Y. Takagi, Note on ferroelectric domain switching, J. Phys. Soc. Jpn. **31**, 506 (1971).
[17] S. Hirata and T. Tako, Temporally ordered structure of a nematic liquid crystal, J. Phys. Soc. Jpn. **51**, 2405 (1982).
[18] A. Joets and R. Ribotta, Localized bifurcations and defect instabilities in the convection of a nematic liquid crystal, J. Stat. Phys. **64**, 981 (1991).
[19] M. Sano, H. Kokubo, B. Janiaud, and K. Sato, Phase wave in a cellular structure, Prog. Theor. Phys. **90**, 1 (1993).
[20] Y. Hidaka, M. Hashiguchi, N. Oikawa, and S. Kai, Lagrangian chaos and particle diffusion in electroconvection of planar nematic liquid crystals, Phys. Rev. E **92**, 032909 (2015).
[21] Y. Hidaka, K. Ijigawa, S.-Y. Kwak, N. Oikawa, H. Okabe, and K. Hara, Information reduction for chaotic patterns, Forma **33**, S3 (2018).
[22] Areas of the pre-GP mentioned below are not counted as the GP area since its wave number is different from q_{GP}.
[23] E. Bodenschatz, W. Zimmermann, and L. Kramer, On electrically driven pattern-forming instabilities in planar nematics, J. Phys. (France) **49**, 1875 (1988).
[24] Y. Hidaka, H. Orihara, and Y. Ishibashi, The transition from quasi-periodicity to chaos in the electro-hydrodynamic instability of a nematic liquid crystal, J. Phys. Soc. Jpn. **61**, 3950 (1992).
[25] S. Nasuno, O. Sasaki, and S. Kai, Secondary instabilities in electroconvection in nematic liquid crystals, Phys. Rev. A **46**, 4954 (1992).
[26] S. Kai, M. Kohno, M. Andoh, M. Imasaki, and W. Zimmermann, Defect dynamics and statistics of defect chaos in electrohydrodynamic convections in nematics, Mol. Cryst. Liq. Cryst. **198**, 247 (1991).
[27] N. Éber, P. Salamon, and Á. Buka, Electrically induced patterns in nematics and how to avoid them, Liq. Cryst. Rev. **4**, 101 (2016).
[28] T. Narumi, Y. Mikami, T. Nagaya, H. Okabe, K. Hara, and Y. Hidaka, Relaxation with long-period oscillation in defect turbulence of planar nematic liquid crystals, Phys. Rev. E **94**, 042701 (2016).
[29] E. Plaut and W. Pesch, Extended weakly nonlinear theory of planar nematic convection, Phys. Rev. E **59**, 1747 (1998).
[30] N. Oikawa, Y. Hidaka, and S. Kai, Formation of a defect lattice in electroconvection of nematics, Phys. Rev. E **70**, 066204 (2004).
[31] P. Le Gal, A. Pocheau, and V. Croquette, Square Versus Roll Pattern at Convective Threshold, Phys. Rev. Lett. **54**, 2501 (1985).
[32] E. Moses and V. Steinberg, Competing Patterns in a Convective Binary Mixture, Phys. Rev. Lett. **57**, 2018 (1986).
[33] S. Ciliberto and P. Bigazzi, Spatiotemporal Intermittency in Rayleigh-Bénard Convection, Phys. Rev. Lett. **60**, 286 (1988).
[34] P. Rupp, R. Richter, and I. Rehberg, Critical exponents of directed percolation measured in spatiotemporal intermittency, Phys. Rev. E **67**, 036209 (2003).
[35] K. Kaneko, Spatiotemporal intermittency in coupled map lattices, Prog. Theor. Phys. **74**, 1033 (1985).

[36] H. Chaté and P. Manneville, Transition to Turbulence Via Spatio-Temporal Intermittency, Phys. Rev. Lett. **58**, 112 (1987).

[37] K. A. Takeuchi, M. Kuroda, H. Chaté, and M. Sano, Directed Percolation Criticality in Turbulent Liquid Crystals, Phys. Rev. Lett. **99**, 234503 (2007).

[38] K. A. Takeuchi, Experimental approaches to universal out-of-equilibrium scaling laws: Turbulent liquid crystal and other developments, J. Stat. Mech. (2014) P01006.

[39] M. Sano and K. Tamai, A universal transition to turbulence in channel flow, Nat. Phys. **12**, 249 (2016).

[40] G. Lemoult, L. Shi, K. Avila, S. V. Jalikop, M. Avila, and B. Hof, Directed percolation phase transition to sustained turbulence in Couette flow, Nat. Phys. **12**, 254 (2016).

[41] O. Al Hammal, H. Chaté, I. Dornic, and M. A. Muñoz, Langevin Description of Critical Phenomena with Two Symmetric Absorbing States, Phys. Rev. Lett. **94**, 230601 (2005).